

Abstract

The wave patterns that occur when a shock wave interacts with an abrupt area change are analyzed in terms of the incident shock wave Mach number and area-jump ratio. The solutions predicted by a self-similar model are in good agreement with those obtained numerically from the quasi-one-dimensional time-dependent Euler equations. The entropy production for the wave system is defined and the principle of minimum entropy production is used to resolve a nonuniqueness problem of the self-similar model.

Introduction

The interaction of a shock wave with a channel of rapidly varying cross-sectional area is of interest in a number of practical problems, such as the passage of shocks through wire-mesh screens, the starting process in a supersonic wind tunnel, and the phenomena that occur in piston engines and jet engines. Previous investigators (refs. 1–3) have shown that a self-similar inviscid model with a discontinuous area change can provide good agreement with experimental observations. A solution to this model is obtained by guessing a self-similar wave pattern with its origin at the location of the area discontinuity. The guessed pattern is validated if the conservation laws of mass, momentum, and energy can be satisfied. The problem essentially depends on two parameters: the strength of the incident shock wave, measured by the shock wave Mach number, and the area ratio across the discontinuity. This parameter space is rich in the number of possible wave patterns and several investigators (refs. 3–5) have indicated that more than one wave pattern might satisfy all the conservation laws.

The existence of multiple solutions was the subject of an article by Oppenheim, Urtiew, and Stern (ref. 5). They showed that, in a region of the parameter space corresponding to supersonic flow behind the incident shock and within a certain range of area contraction, three wave patterns could satisfy all the conservation laws. Oppenheim, Urtiew, and Stern conjectured that the ambiguity could be resolved by invoking the minimum entropy production principle. This led them to accept two solutions in this region, one with a standing shock wave within the area contraction. Rudinger (refs. 6 and 7) questioned their conclusion, pointing to the well known fact that a standing shock in a converging channel is unstable. Through a study of the transient phenomena produced by a steep, but continuous, area variation, Rudinger concluded that the only solution that could be realized in this ambiguous region corresponds to a wave pattern with a rarefaction swept downstream. Here we show that the solution pro-

posed by Rudinger can be reconciled with the minimum entropy production principle if the entropy production is properly defined.

Rudinger's transient analysis was based on a graphical method of characteristics. This tedious approach limited Rudinger to the study of three specific examples. In order to establish conclusively that a reflected shock wave cannot be formed in the region of ambiguity, Rudinger proceeded to show that the waves reflected from the transmitted shock cannot coalesce until the head of the reflected wave becomes stationary, that is, the flow becomes sonic. Implicit in the proof is the assumption that the head of the reflected wave becomes stationary for conditions on one of the boundaries of the region of ambiguity. While this is true for the self-similar model, it is not clear that this is also true for the transient problem.

For an area divergence, no multiple solutions are known to exist. The region of ambiguity that occurs for an area contraction can be shown to extend into the region corresponding to an area divergence in parameter space. Here, however, a unique solution with a standing shock is found.

The purpose of this paper is to map the different wave patterns that take place for the self-similar model in terms of the incident shock strength and area ratio and to verify the validity of these solutions by solving the time-dependent quasi-one-dimensional Euler equations for flow in a channel with a steep cross section. The study is limited to monotonically increasing or decreasing areas. The problem is defined and its method of solution is explained in the first section. This section also investigates the flow patterns that take place for an area divergence and an area contraction. Following in the next section, the quasi-one-dimensional model is introduced and the numerical method for solving this problem is outlined. The results section compares the self-similar model and the quasi-one-dimensional model. Finally, conclusions are discussed in the last section.

Symbols

A	channel area	z	argument for minmod limiter
A_L	channel area to the left of area discontinuity	α	area ratio (see eq. (1))
A_R	channel area to the right of area discontinuity	α_c	asymptote of curve c (see fig. 2)
a	speed of sound	α_d	asymptote of curve d (see fig. 2)
C	Riemann variable defined by equation (21)	β	defined by equation (25)
D	Jacobian matrix defined by equation (27)	γ	specific heat ratio
e	specific total energy	δ	defined by equation (4)
F	flux matrix defined by equation (24)	κ	defined by equation (4)
K	constant in minmod limiter	λ	characteristic slope
L_U	left eigenvector matrix of C	ν	constant appearing in minmod limiter
M	Mach number	ρ	density
M_i^*	value of M_i corresponding to sonic conditions in region 3	σ	constant appearing in equation (22)
p	pressure	χ	entropy production
p_r	pressure ratio (see eq. (9))	Subscripts:	
Q	source vector defined by equation (24)	i	incident shock
R	residual defined by equation (33)	k	time counter
S	entropy (see eq. (5))	n	space counter
t	time	r	reflected shock
U	unknown vector defined by equation (24)	t	transmitted shock; differentiation with respect to time
u	velocity	x	differentiation with respect to x
W	characteristic variable vector defined by equation (28)	0	starting conditions
\widetilde{W}	value of W returned by minmod limiter	1, 2, 3, ...	regions of flow
w	shock wave speed	Superscripts:	
x	axial coordinate	k	time counter
y	argument for minmod limiter	+	forward difference
		−	backward difference
		()	Runge-Kutta stage
		Special notation:	
		a, b, \dots, e	curves in figure 2
		I, II, ..., IV	quadrants in figure 2
		Ia, Ib, Ic, IIa, IIb, IIIa, IIIb, IVa	flow patterns in quadrants

Self-Similar Model

Consider two infinitely long constant area ducts that are connected by a short, monotonically increasing or decreasing transition section. Assume that the transition section is small enough that it can be replaced by an abrupt transition. Further assume that the gas inside the duct is at rest. We are interested in establishing the valid wave patterns that result when a shock wave moving from left to right passes through the discontinuous area change. Let $x = 0$ be the location of the area jump, and let $t = 0$ be the time at which the incident shock reaches the area jump. Because there is no reference length, we expect the solution to be constant along rays originating at $(0,0)$. That is, the dependent variables are only functions of the ratio x/t .

Method of Solution

A typical wave diagram of the interaction of a shock wave with an area discontinuity is shown in figure 1. In all such figures that follow, the area discontinuity is depicted as a long-dash line, the shock waves are depicted as thick solid lines, a contact surface is depicted as a short-dash line, and an expansion fan is depicted by thin solid lines. Region 1 is the region to the right of the area discontinuity and ahead of the transmitted shock; region 2 is the region to the left of the area discontinuity and ahead of the incident shock. The flow is assumed to be at rest in both of these regions, and the pressure and density are assumed to be uniform. The pattern shown in figure 1 is one of many that we will be discussing later. The flow conditions leading to this pattern correspond to a high incident shock Mach number and a high area ratio. The area ratio α is defined as

$$\alpha = \frac{A_L}{A_R} \quad (1)$$

where A_L is the area to the left and A_R is the area to the right, both assumed to have a nondimensional length of 1.

The conditions in region 3, immediately behind the incident shock, are evaluated from the Rankine-Hugoniot relations:

$$\left. \begin{aligned} u_3 &= \frac{a_2 (M_i^2 - 1)}{\kappa M_i} \\ \rho_3 &= \frac{\rho_2 \kappa M_i^2}{(\delta M_i^2 + 1)} \\ p_3 &= p_2 \frac{\gamma M_i^2 - \delta}{\kappa} \end{aligned} \right\} \quad (2)$$

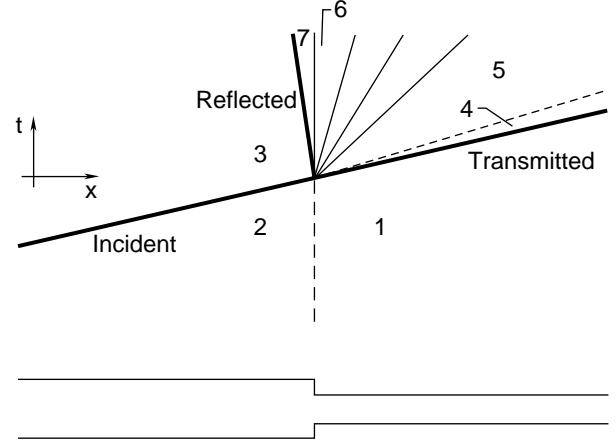


Figure 1. Typical wave diagram for the interaction of a shock with an area discontinuity.

Here, u , ρ , a , and p are the velocity, density, speed of sound, and pressure, respectively. Pressure and density are nondimensionalized by their initial values in region 1, and all velocities are nondimensionalized by the speed of sound in region 1 divided by $\sqrt{\gamma}$. The subscripts in equations (2) denote the appropriate region. The Mach number of the incident shock is denoted by M_i and is given by

$$M_i = \frac{w_i}{a_2} \quad (3)$$

where w_i is the incident shock speed. In the following, δ and κ are given by

$$\left. \begin{aligned} \delta &= \frac{\gamma - 1}{2} \\ \kappa &= \frac{\gamma + 1}{2} \end{aligned} \right\} \quad (4)$$

From the definitions of the speed of sound and the entropy, we have

$$\left. \begin{aligned} a_3 &= \sqrt{\frac{\gamma p_3}{\rho_3}} \\ S_3 &= \ln(p_3) - \gamma \ln(\rho_3) \end{aligned} \right\} \quad (5)$$

Conditions in regions 1 and 2 are given by

$$\left. \begin{aligned} u_1 &= u_2 = 0 \\ a_1 &= a_2 = \sqrt{\gamma} \\ p_2 &= p_1 = 1 \\ \rho_2 &= \rho_1 = 1 \\ S_2 &= S_1 = 0 \end{aligned} \right\} \quad (6)$$

The flow in region 3 becomes sonic when M_i equals some critical value M_i^* . If we set $M_3 = 1$, using equations (2) and (5), we get

$$M_i^{*2} = \frac{(7 - \gamma) + \sqrt{(7 - \gamma)^2 - 16(2 - \gamma)}}{4(2 - \gamma)} \quad (7)$$

For values of M_i greater than M_i^* , the flow in region 3 is supersonic. For $\gamma = 1.4$, $M_i^* = 2.068$. As $M_i \rightarrow \infty$, the Mach number in region 3 approaches the value $1/\sqrt{\gamma\delta}$. For $\gamma = 1.4$, the upper limit for M_3 is 1.890.

Across the contact surface, the following two relations must be satisfied:

$$\left. \begin{aligned} p_4 &= p_5 \\ u_4 &= u_5 \end{aligned} \right\} \quad (8)$$

If the Mach number M_t of the transmitted shock is known, then the flow in region 4 is defined by equations (2) and (5), with M_i replaced by M_t and subscripts 2 and 3 replaced by 1 and 4, respectively. The Mach number of the transmitted shock, in terms of the pressure ratio $p_r = p_4/p_1$, is given by

$$M_t = \sqrt{\frac{\kappa p_r + \delta}{\gamma}} \quad (9)$$

Therefore, with p_5 known, region 4 is completely defined.

In general, the wave pattern between regions 3 and 5 will be different from that shown in figure 1. The specific pattern will depend on the value of the incident Mach number and the area ratio. Here we illustrate how the solution for the wave pattern of figure 1 is obtained, with the understanding that similar procedures are used as the wave pattern changes between regions 3 and 5.

The Mach number in region 6 (region 6 is actually one point in space), immediately to the right of the area discontinuity, is sonic. Therefore, by solving the conservation of mass relation written in the form

$$\alpha = \frac{M_6}{M_7} \left(\frac{1 + \delta M_7^2}{1 + \delta M_6^2} \right)^{\kappa/2\delta} \quad (10)$$

we can obtain M_7 . Given M_7 , the Rankine-Hugoniot relations across the reflected shock can be solved iteratively to obtain the solution for region 7. With region 7 defined, we turn our attention again to region 6. Since the flow is isentropic between regions 7 and 6, we have

$$S_6 = S_7 \quad (11)$$

From the conservation of total enthalpy,

$$a_6 = a_7 \left(\frac{1 + \delta M_7^2}{\kappa} \right)^{1/2} \quad (12)$$

and since the flow is sonic in region 6,

$$u_6 = a_6 \quad (13)$$

The density and pressure follow from equations (5):

$$\left. \begin{aligned} \rho_6 &= \exp \left[\frac{\ln(a_6^2/\gamma) - S_6}{2\delta} \right] \\ p_6 &= \frac{\rho_6 a_6^2}{\gamma} \end{aligned} \right\} \quad (14)$$

The Riemann variable on the characteristic with slope $u + a$, crossing the expansion fan, provides one piece of information about region 5. If we guess the slope of the expansion tail, $\lambda_5 = u_5 - a_5$, after some simplification we get

$$\left. \begin{aligned} u_5 &= a_6 + \frac{\lambda_5}{\kappa} \\ a_5 &= u_5 - \lambda_5 \end{aligned} \right\} \quad (15)$$

Because $S_5 = S_6$, the pressure and density in region 5 can be obtained from equations (14) with an appropriate change of subscripts. If u_5 matches u_4 the problem is solved. Otherwise, we continue iterating on λ_5 until $u_5 = u_4$.

The lines $M_i = 2.068$ and $\alpha = 1$ lead to a natural breakup of the parameter space M_i, α into four quadrants, as shown in figure 2. In the following two sections, we explore the various wave patterns that represent solutions in each of these quadrants.

Area Divergence

Consider the first quadrant, $M_i < 2.068$ and $\alpha < 1$. For weak incident shocks, a weak rarefaction wave is reflected when the shock crosses the area discontinuity. The effect of the rarefaction is to accelerate the flow before it enters into the area divergence. Because the flow remains subsonic as it reaches the area divergence, it is decelerated as it crosses into the big chamber. In general the transmitted shock is weaker than the incident shock. Figure 3 shows the wave pattern that is valid in this region, which we label Ia. The flow conditions for this figure are $M_i = 1.100$ and $\alpha = 0.5$.

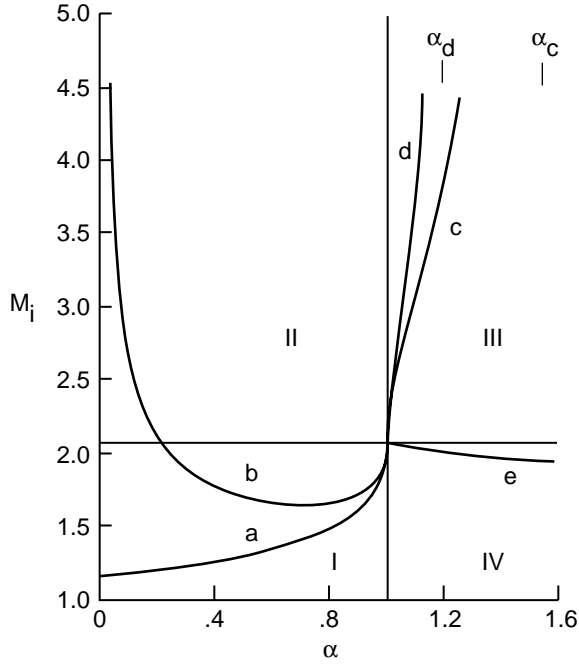


Figure 2. Parameter space M_i, α .

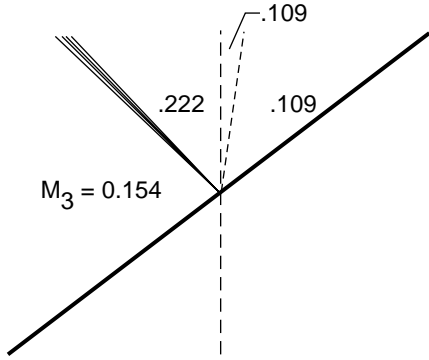


Figure 3. Wave pattern Ia. $M_i = 1.100$; $\alpha = 0.5$.

As the strength of the incident shock increases, the rarefaction wave becomes stronger, eventually creating sonic conditions at the entrance to the area divergence. The locus of points corresponding to sonic conditions at the entrance to the divergence is shown as curve *a* in figure 2. The wave pattern along this curve is of type Ia. Figure 4 shows the pattern for $M_i = 1.303$ and $\alpha = 0.5$. If $\alpha \rightarrow 0$, curve *a* approaches asymptotically a value of 1.154 for $\gamma = 1.4$.

If the shock strength continues to increase, a standing shock develops where the area jumps. If we model the area change by a continuous variation,

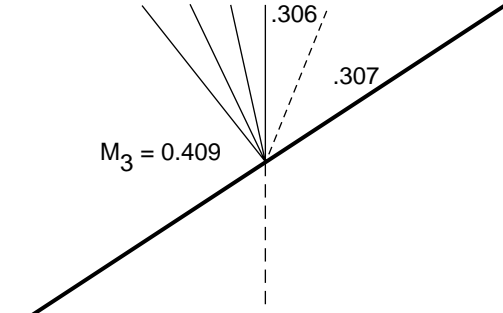


Figure 4. Wave pattern along curve *a*, type Ia. $M_i = 1.303$; $\alpha = 0.5$.

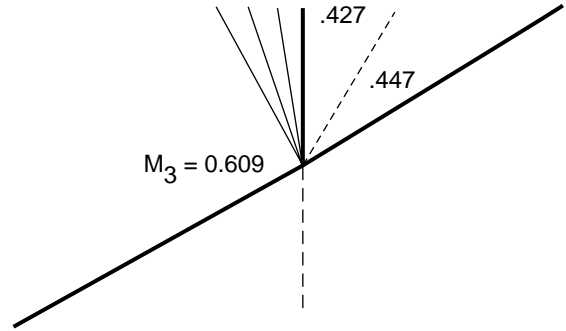


Figure 5. Wave pattern Ib. $M_i = 1.500$; $\alpha = 0.5$.

then as the incident shock strength increases, the standing shock becomes stronger and moves from the entrance of the divergence, where the area is A_L , to the exit, where the area is A_R . If the area change is modeled by a discontinuity, the standing shock has no distance to move as the incident shock gains strength. The shock motion can only be accounted for through a change in the Mach number ahead of the shock. This in effect models the shock motion between A_L and A_R . Figure 5 shows wave pattern Ib corresponding to a standing shock wave. The conditions for this case are $M_i = 1.500$ and $\alpha = 0.5$. The Mach number immediately ahead of the divergence is sonic. From sonic conditions, the flow is isentropically accelerated to Mach 1.927, corresponding to an area ratio of 0.629. After the flow crosses the standing shock, the Mach number becomes 0.591. The flow is then isentropically compressed to Mach 0.427, corresponding to an area ratio of 0.794. This completes the overall area divergence ratio of 0.5. A discontinuous area change causes a squeeze of all these Mach number jumps into one point in space.

As the shock strength continues to increase, the standing shock reaches the exit of the area divergence. At this point, the flow in front of the shock

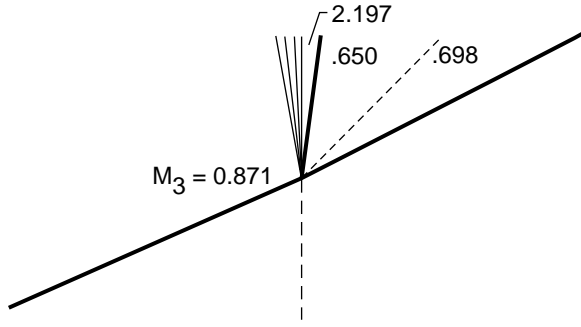


Figure 6. Wave pattern Ic. $M_i = 1.850$; $\alpha = 0.5$.

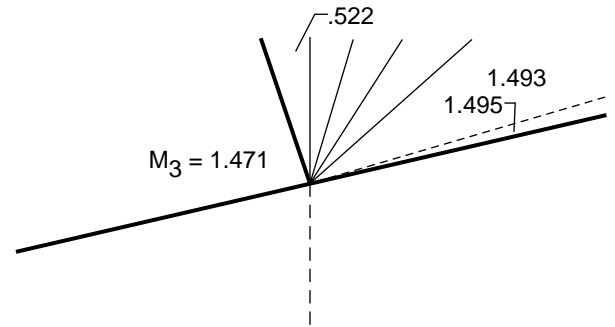


Figure 8. Wave pattern IIIa. $M_i = 3.500$; $\alpha = 1.3$.

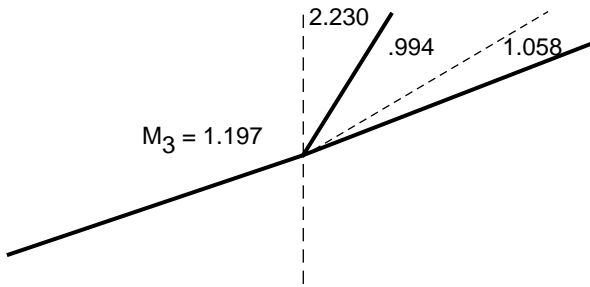


Figure 7. Wave pattern IIa. $M_i = 2.500$; $\alpha = 0.5$.

goes through an isentropic expansion corresponding to the full area jump. The locus of points corresponding to this condition maps to curve *b* in figure 2.

The wave pattern changes to type Ic with a further increase in shock strength. Now the standing shock is swept downstream, the result being the pattern shown in figure 6 for $M_i = 1.850$ and $\alpha = 0.5$. This pattern occurs in the region bounded by curve *b* and line $M_i = M_i^*$. Above curve *b*, the flow entering the big chamber is supersonic. As M_i approaches M_i^* the reflected expansion fan disappears.

Consider the second quadrant, $M_i > 2.068$ and $\alpha < 1$. In this quadrant the flow behind the incident shock is supersonic. For area ratios to the right of curve *b* the pattern that occurs is shown in figure 7. The figure is drawn for $M_i = 2.500$ and $\alpha = 0.5$. The significant features of this pattern, labeled IIa, are the absence of a reflected wave and the appearance of a downstream running secondary shock. As discussed previously, the Mach number behind the incident shock is bounded by the value 1.890 for $\gamma = 1.4$. This Mach number limitation does not apply to the flow to the right of the area divergence. Here very high Mach numbers can be achieved by decreasing the area ratio α , but keeping it to the right of curve *b*. For example, for the conditions of figure 7, Mach 2.230 is achieved in the big chamber. If the area ratio for this case is lowered to 0.15, Mach 3.512 is achieved in the big

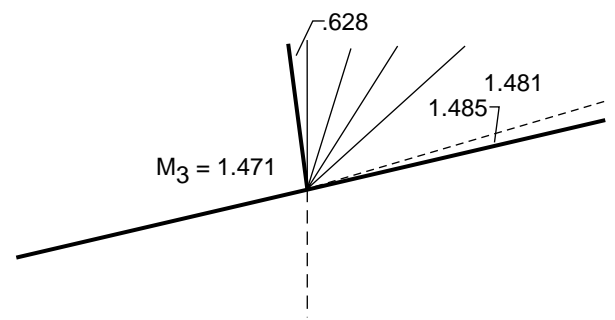


Figure 9. Wave pattern along curve *c*, type IIIa. $M_i = 3.500$; $\alpha = 1.157$.

chamber. This fact was used by Hertzberg (ref. 8) to design a new shock tube for hypersonic flows. If, at a given M_i , the area ratio is less than or equal to the ratio corresponding to curve *b*, then the secondary shock becomes a standing shock. This pattern is labeled IIb. It is very similar to pattern Ib, figure 5, except that the flow behind the incident shock is supersonic and there is no reflected rarefaction wave.

Area Contraction

Consider the third quadrant, $M_i > 2.068$ and $\alpha > 1$. If the area ratio is large, wave pattern IIIa occurs. This is illustrated in figure 8 for $M_i = 3.500$ and $\alpha = 1.3$. In this region the reflected wave is a shock. The subsonic flow behind the reflected shock is accelerated to sonic conditions by the area convergence. The flow is then further accelerated by a rarefaction wave running downstream. In general, the transmitted shock is stronger than the incident shock. If we decrease the area ratio, holding M_i fixed, we reach curve *c* of figure 2 when $\alpha = 1.157$. The wave pattern at these conditions is illustrated in figure 9. It is clearly a type IIIa pattern. If we continue to decrease the area ratio, holding M_i , we reach curve *d* when $\alpha = 1.086$. At these conditions the reflected shock becomes a standing shock, which

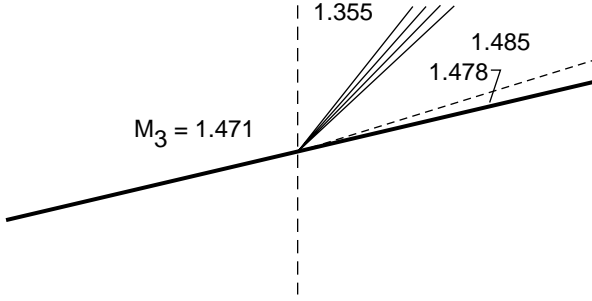


Figure 10. Wave pattern IIIb. $M_i = 3.500$; $\alpha = 1.06$.

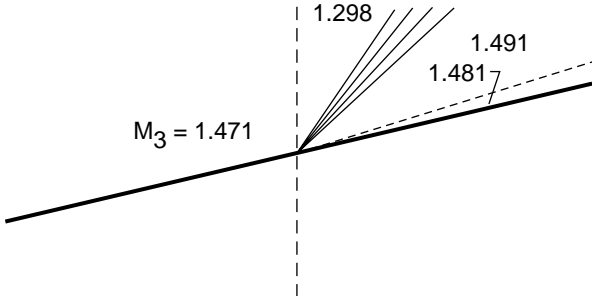


Figure 11. Wave pattern along curve d , type IIIb. $M_i = 3.500$; $\alpha = 1.086$.

is the limiting case of pattern IIIa. Curve d consists of the locus of points for which the reflected shock becomes a standing shock. Oppenheim, Urtiew, and Stern (ref. 5) showed that as $M_i \rightarrow \infty$, curve d approaches an area ratio α_d given by

$$\alpha_d = \frac{1}{\sqrt{2\delta}} [\gamma(1 - \delta)]^{-1/2\delta} \quad (16)$$

For $\gamma = 1.4$, α_d takes on the value 1.543.

If the area ratio is just slightly greater than one, then we have a type IIIb wave pattern. This wave pattern is illustrated in figure 10 for $M_i = 3.500$ and $\alpha = 1.06$. Under these conditions, the flow reaches the area jump at supersonic speed. The area contraction compresses the flow isentropically, but not sufficiently to make the flow subsonic. Once within the small chamber, the flow is accelerated by a rarefaction wave running downstream. If we hold M_i fixed and increase the area ratio, we reach curve d when $\alpha = 1.086$. The wave pattern is illustrated in figure 11 and is clearly a type IIIb pattern. If we further increase the area ratio, we reach curve c when $\alpha = 1.157$. At these conditions, the area ratio isentropically compresses the supersonic flow behind the incident shock to sonic conditions. Thus, the head of the expansion running downstream in

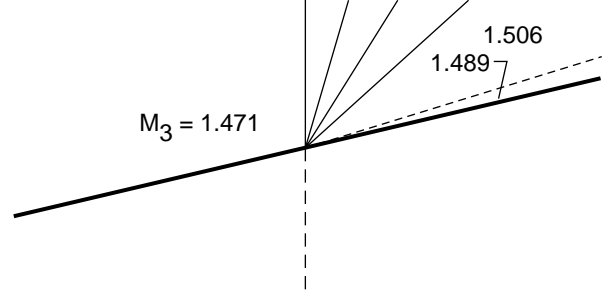


Figure 12. Wave pattern along curve c , type IIIb. $M_i = 3.500$; $\alpha = 1.157$.

the small chamber is sonic. This wave pattern is illustrated in figure 12. Curve c represents the locus of points for which the area ratio produces sonic conditions after the area jump. Oppenheim, Urtiew, and Stern (ref. 5) also showed that as $M_i \rightarrow \infty$, curve c approaches an area ratio α_c given by

$$\alpha_c = \sqrt{2\delta} \left(\frac{\gamma}{2}\right)^{-1/2\delta} \quad (17)$$

For $\gamma = 1.4$, α_c takes on the value 1.193.

The region between curves c and d is the region of ambiguity discussed by Oppenheim, Urtiew, and Stern (ref. 5) and Rudinger (refs. 6 and 7). As we have already seen, wave patterns IIIa and IIIb coexist in this region. In addition, a third pattern with a standing shock within the area contraction and an expansion running downstream is also a solution of the self-similar model.

Oppenheim, Urtiew, and Stern (ref. 5) invoked the principle of minimum entropy production to resolve the ambiguity. For each solution in this region they defined the entropy production χ to be

$$\chi = \max(S_4, S_5) \quad (18)$$

The resulting entropy production is shown in figure 13 for $M_i = 3.500$ and $1.086 \leq \alpha \leq 1.157$. From this, they concluded that wave pattern IIIb was valid for area ratios slightly greater than those on curve d . However, at some point within the region of ambiguity the standing shock pattern would take over until curve c was reached. Rudinger (ref. 6) objected to their conclusion, dismissing outright the minimum entropy principle and correctly pointing out that for an area contraction a standing shock solution is unstable, as has also been shown in other investigations (ref. 9). Rudinger (refs. 6 and 7) further showed that if the area discontinuity is replaced by a steep area

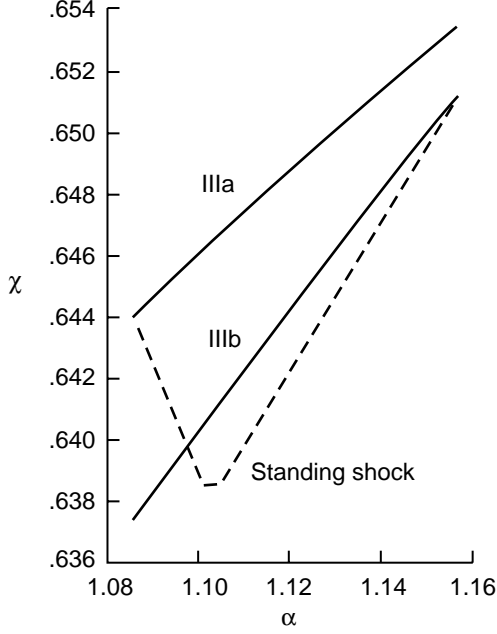


Figure 13. Entropy production in region of ambiguity. (Based on Oppenheim, Urtiew, and Stern (ref. 5).)

variation and a time-dependent analysis of the shock-area interaction is carried out, the wave pattern observed within the ambiguity region is IIIb.

The minimum entropy production principle failed to predict the valid solution because the entropy production was incorrectly defined. The total entropy of an infinitesimal element of mass is $S\rho A dx$. If we integrate between $x = -\infty$ and $x = \infty$ at a fixed time t , we get the total entropy in the channel. The entropy production in an interval of time Δt is, therefore, given by

$$\chi = \int_{-\infty}^{\infty} [\rho(\Delta t)S(\Delta t) - \rho(0)S(0)] A dx \quad (19)$$

Equation (19) can be easily integrated in closed form. For wave pattern IIIa, figure 8, we get

$$\begin{aligned} \frac{\chi}{\Delta t} = & (\rho_3 S_3 - \rho_7 S_7) w_r + \frac{S_5}{\alpha} \int_0^{u_5 - a_5} \rho dx \\ & + \frac{1}{\alpha} [\rho_5 S_5 a_5 + \rho_4 S_4 (w_t - u_4)] \end{aligned} \quad (20)$$

Region 7 is downstream of the reflected shock, and w_r and w_t are the speeds of the reflected and transmitted shocks, respectively. The remaining integral

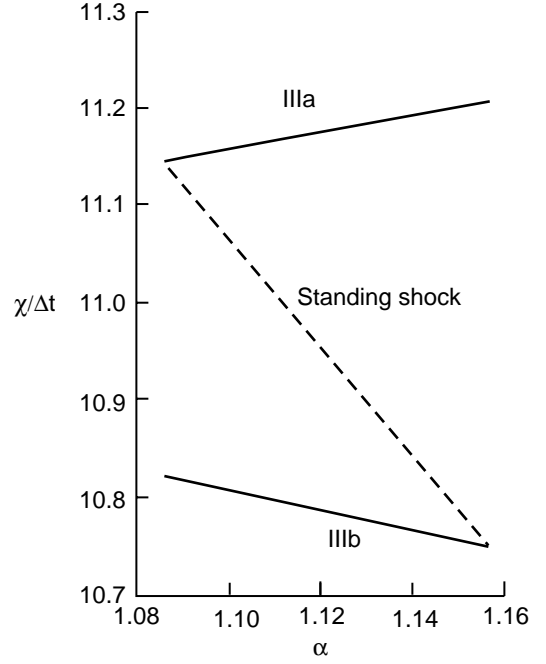


Figure 14. Entropy production in region of ambiguity.

in equation (20) integrates to

$$\left. \begin{aligned} \int_0^{u_5 - a_5} \rho dx = & \left[\frac{\exp(-S_5)}{\gamma} \left(\frac{\delta}{\kappa} \right)^2 \right]^{1/2\delta} \\ & \times \left[C^{k/\delta} - (C - u_5 + a_5)^{k/\delta} \right] \frac{\delta}{\kappa} \\ C = & \frac{a_6}{\delta} + u_6 \end{aligned} \right\} \quad (21)$$

With similar results for the other two wave patterns, we obtain figure 14. Now, the standing shock solution links patterns IIIa and IIIb without overlapping pattern IIIb, and the latter produces the minimum entropy consistent with Rudinger's time-dependent computations. The figure also shows that the transition between pattern IIIb and IIIa across curve c is discontinuous.

If we consider the wave patterns along curves a and c , figures 4 and 12, we see that the patterns are very similar, and we can think of curve c as the extension of curve a into the third quadrant. The same can be said of curves b and d . Curve d is not a boundary between two different wave patterns and, now that the ambiguity has been resolved, it could be disregarded.

Consider the fourth quadrant, $M_i < 2.068$ and $\alpha > 1$. Here we find wave pattern IVa, illustrated in figure 15 for $M_i = 1.500$ and $\alpha = 1.3$. The

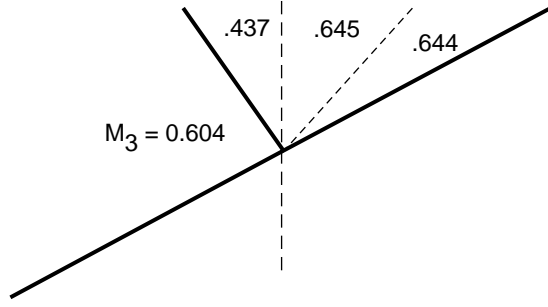


Figure 15. Wave pattern IVa. $M_i = 1.500$; $\alpha = 1.3$.

salient features are a reflected shock moving into the subsonic flow behind the incident shock and an isentropic acceleration of the flow entering the area contraction not sufficiently strong to generate supersonic flow in the small chamber. If we hold α fixed and increase M_i , curve e is met when M_i reaches the value 1.988. At this point the flow in the small chamber reaches sonic conditions. Curve e , thus, is the locus of points separating patterns IIIa and IVa. If $\alpha \rightarrow \infty$, curve e approaches asymptotically a value of 1.718 for $\gamma = 1.4$.

Quasi-One-Dimensional Time-Dependent Model

In this formulation, the discontinuous area jump is replaced by a steep area change defined by

$$A(x) = \frac{1}{2}(A_L + A_R) - \frac{1}{2}(A_L - A_R) \tanh(\sigma x) \quad (22)$$

The transition from A_L to A_R is centered about $x = 0$ and takes place in an interval approximately equal to $2/\sigma$.

Inside the duct defined by equation (22) we solve the quasi-one-dimensional Euler equations in weak conservation form

$$\mathbf{U}_t + \mathbf{F}_x = \mathbf{Q} \quad (23)$$

where

$$\mathbf{U} = \begin{Bmatrix} \rho \\ \rho u \\ \rho e \end{Bmatrix} \mathbf{F} = \begin{bmatrix} \rho u \\ p + \rho u^2 \\ u(\rho e + p) \end{bmatrix} \mathbf{Q} = \begin{Bmatrix} \rho u \beta \\ \rho u^2 \beta \\ u(\rho e + p) \beta \end{Bmatrix} \quad (24)$$

and

$$\left. \begin{aligned} p &= \delta \rho (2e - u^2) \\ \beta &= \frac{A_x}{A} \end{aligned} \right\} \quad (25)$$

The quasi-linear form of equation (23) is

$$\mathbf{U}_t + \mathbf{D}(\mathbf{U})\mathbf{U}_x = \mathbf{Q} \quad (26)$$

where

$$\mathbf{D}(\mathbf{U}) = \frac{\partial \mathbf{F}}{\partial \mathbf{U}} = \begin{bmatrix} 0 & 1 & 0 \\ \frac{1}{2}(\gamma - 3)u^2 & (3 - \gamma)u & 2\delta \\ 2\delta u^3 - \gamma u e/p & \gamma e/p - 3\delta u^2 & \gamma u \end{bmatrix} \quad (27)$$

We introduce a discrete grid $(x_n, t_k) = (x_0 + n \Delta x, t_0 + k \Delta t_k)$ where Δx is constant, but Δt_k changes from time step to time step to satisfy the CFL condition (ref. 10). On this grid, we obtain an approximation to our dependent variable \mathbf{U} at cell centers $x_n + \frac{1}{2}\Delta x$ using the Roe scheme (ref. 11) to approximate the flux derivative in equation (23). In the original Roe scheme, the dependent variable \mathbf{U} is interpolated to the cell faces. In our implementation, we first construct the characteristic differences ΔW^\pm from

$$\Delta \mathbf{W}^\pm = \mathbf{L}_U \Delta \mathbf{U}^\pm \quad (28)$$

where

$$\left. \begin{aligned} \Delta \mathbf{U}^+ &= \mathbf{U}_{n+1} - \mathbf{U}_n \\ \Delta \mathbf{U}^- &= \mathbf{U}_n - \mathbf{U}_{n-1} \end{aligned} \right\} \quad (29)$$

and \mathbf{L}_U is the left eigenvector matrix of $\mathbf{D}(\mathbf{U})$ evaluated with \mathbf{U}_n values. The characteristic difference is then limited using the minmod limiter

$$\left. \begin{aligned} \Delta \widetilde{\mathbf{W}}^\pm &= \text{minmod} \left[\Delta \mathbf{W}^\pm, \nu \Delta \mathbf{W}^\mp \right] \\ \nu &= \frac{3 - K}{1 - K} \end{aligned} \right\} \quad (30)$$

where

$$\text{minmod}[z, y] = \begin{cases} 0 & \text{sign}(z) \neq \text{sign}(y) \\ \text{sign}(z) \min(|z|, |y|) & \text{sign}(z) = \text{sign}(y) \end{cases} \quad (31)$$

and K is the free constant in the kappa interpolation of van Leer (ref. 12), which we use to interpolate $\Delta \widetilde{\mathbf{W}}$ to the cell faces. In this application $K = 1/3$. At the cell faces $\Delta \mathbf{U}$ is reconstructed from

$$\Delta \mathbf{U} = \mathbf{L}_U^{-1} \Delta \widetilde{\mathbf{W}} \quad (32)$$

The additional work to construct the characteristic differences and then the conservative variables was required in order to capture a strong shock. Without this work, the algorithm produces large oscillations and eventually fails. The rest of the flux evaluation

follows the Roe scheme as described in reference 11.

Equation (23) is integrated in time using a three-stage Runge-Kutta scheme. Let

$$\mathcal{R}(\mathbf{U}) = \Delta t_k (\mathbf{Q} - \mathbf{F}_x) \quad (33)$$

then \mathbf{U} at time level $k + 1$ follows from

$$\left. \begin{aligned} \mathbf{U}^{(0)} &= \mathbf{U}^k \\ \mathbf{U}^{(1)} &= \mathbf{U}^{(0)} + \frac{1}{3} \mathcal{R}(\mathbf{U}^{(0)}) \\ \mathbf{U}^{(2)} &= \mathbf{U}^{(0)} + \frac{1}{2} \mathcal{R}(\mathbf{U}^{(1)}) \\ \mathbf{U}^{(3)} &= \mathbf{U}^{(0)} + \mathcal{R}(\mathbf{U}^{(2)}) \\ \mathbf{U}^{k+1} &= \mathbf{U}^{(3)} \end{aligned} \right\} \quad (34)$$

Although the scheme allows a CFL number of 2.8, we have used a CFL number of 1 to avoid wiggles at shock waves. The overall scheme is second order accurate away from discontinuities.

Results

Comparisons between the self-similar model and the quasi-one-dimensional time-dependent model are presented in this section. The integration of the latter is done from $x = -2$ to $x = 2$. The incident shock is located at $x = -0.5$ at $t = 0$. For these cases, $\sigma = 10$ and $\Delta x = 0.02$. The first case is for $M_i = 1.500$ and $\alpha = 0.5$. This case is illustrated in figure 5. It corresponds to a type Ib pattern with a standing shock within the area constriction. The results from the quasi-one-dimensional time-dependent solution are shown in figure 16. The reflected expansion, standing shock, and transmitted shock are clearly shown in the Mach contours. In figure 17, the Mach number distribution at $t = 2.5$ is compared with the levels predicted by the self-similar model. The agreement between the two models is good. For the second comparison, we have chosen conditions corresponding to figure 7, $M_i = 2.500$ and $\alpha = 0.5$. At these conditions, no wave is reflected and a secondary shock running downstream appears. The expected features are clearly shown in the Mach contours in figure 18. The Mach number distribution at $t = 1$ is compared to the self-similar solution in figure 19. The agreement is good except for the slip line in the quasi-one-dimensional time-dependent solution. The slip line is spread over several mesh points. This is a typical problem of shock capturing

Figure 16. Mach number contours from solution to quasi-one-dimensional time-dependent equations for $M_i = 1.500$ and $\alpha = 0.5$.

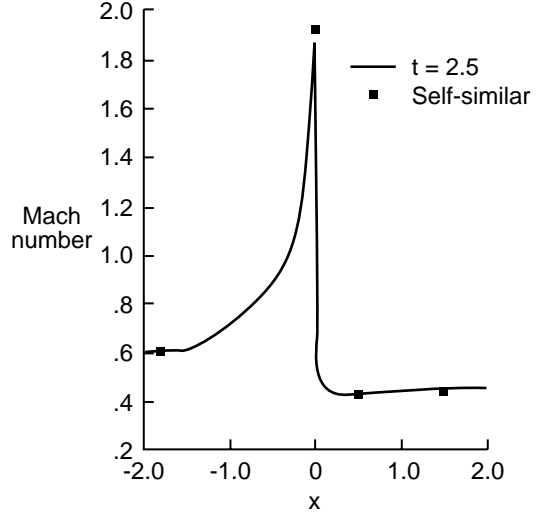


Figure 17. Comparison of self-similar and quasi-one-dimensional time-dependent solutions for $M_i = 1.500$ and $\alpha = 0.5$.

schemes. The third case chosen corresponds to figure 8, $M_i = 3.500$ and $\alpha = 1.3$. This case consists of a reflected shock and a rarefaction wave running downstream. Figure 20 shows the formation of the reflected shock as the left-running characteristics coalesce and the formation of the rarefaction fan from the other family of characteristics. A Mach number cut at $t = 1.4$ is shown in figure 21. The agreement between the two models is good, but the compression

Figure 18. Mach number contours from solution to quasi-one-dimensional time-dependent equations for $M_i = 2.500$ and $\alpha = 0.5$.

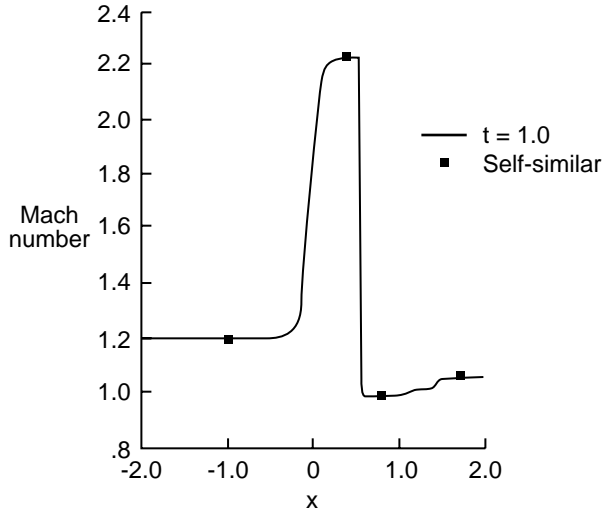


Figure 19. Comparison of self-similar and quasi-one-dimensional time-dependent solutions for $M_i = 2.500$ and $\alpha = 0.5$.

behind the transmitted shock is slightly underpredicted by the quasi-one-dimensional time-dependent solution. For the last case, we have chosen conditions within the region of ambiguity, $M_i = 3.500$ and $\alpha = 1.1$. As predicted by the principle of minimum entropy production, the wave pattern corresponds to pattern IIIb with a rarefaction wave running down-

Figure 20. Mach number contours from solution to quasi-one-dimensional time-dependent equations for $M_i = 3.500$ and $\alpha = 1.3$.

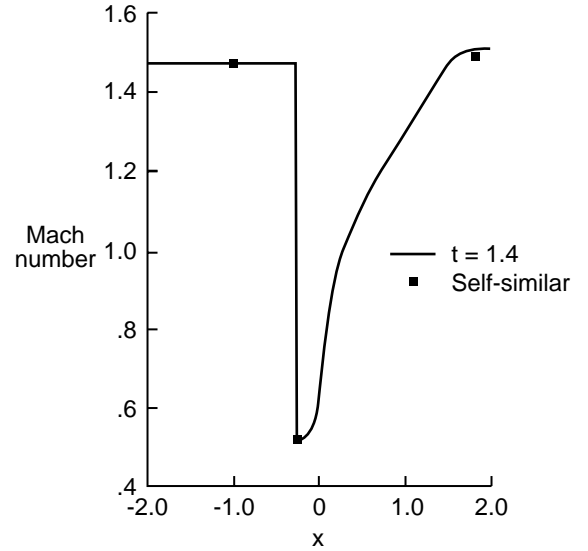


Figure 21. Comparison of self-similar and quasi-one-dimensional time-dependent solutions for $M_i = 3.500$ and $\alpha = 1.3$.

stream. The results are shown in figures 22 and 23. Figure 23 shows that the isentropic recompression produced by the area contraction is properly predicted by the quasi-one-dimensional time-dependent model; however, the expansion running downstream shows a wiggle near its head.

a configuration known to be unstable. The pattern predicted in this region by numerical solutions of the quasi-one-dimensional time-dependent Euler equations is in agreement with earlier results. The entropy produced by the wave system was defined. It was then shown that the admissible pattern in the ambiguous region is in agreement with the predictions of the minimum entropy production principle. This resolved some criticisms of this principle, when applied to this problem, raised by Rudinger. In general, good quantitative agreement was observed between the self-similar model and the quasi-one-dimensional time-dependent model.

NASA Langley Research Center
Hampton, VA 23665-5225
June 18, 1991

Figure 22. Mach number contours from solution to quasi-one-dimensional time-dependent equations for $M_i = 3.500$ and $\alpha = 1.1$.

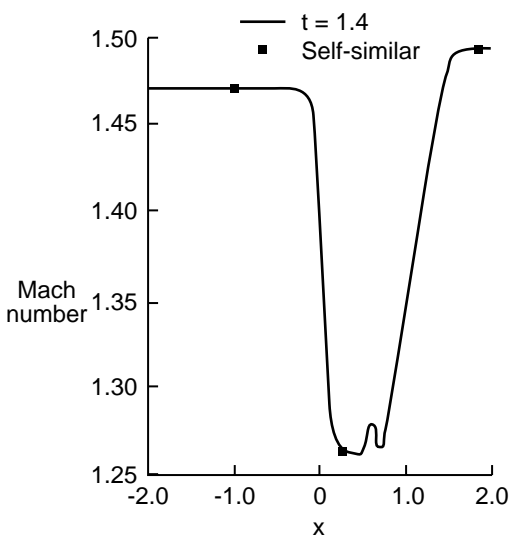


Figure 23. Comparison of self-similar and quasi-one-dimensional time-dependent solutions for $M_i = 3.500$ and $\alpha = 1.1$.

Conclusions

The self-similar model predicted nine wave patterns depending on the incident shock wave Mach number and area-jump ratio. For an area contraction and an incident shock Mach number greater than 2.068, a narrow region was found where three wave patterns satisfy all the governing equations. One of these wave patterns consisted of a standing shock,

References

1. Dosanjh, Darshan S.: Some Comments on "A Theoretical and Experimental Study of Shock Tube Flows." *J. Aeronaut. Sci.*, vol. 22, no. 11, Nov. 1955, pp. 797-799.
2. Franks, W. J.; and Hall, J. Gordon: Collision of Plane Shock Waves With Wire Screens. *J. Aeronaut. Sci.*, vol. 24, no. 12, Dec. 1957, pp. 917-918.
3. Kahane, A.; Warren, W. R.; Griffith, W. C.; and Marino, A. A.: A Theoretical and Experimental Study of Finite Amplitude Wave Interactions With Channels of Varying Area. *J. Aeronaut. Sci.*, vol. 21, no. 8, Aug. 1954, pp. 505-524, 565.
4. Bird, G. A.: The Effect of Wall Shape on the Degree of Reinforcement of a Shock Wave Moving Into a Converging Channel. *J. Fluid Mech.*, vol. 5, pt. 1, Jan. 1959, pp. 60-66.
5. Oppenheim, A. K.; Urtiew, P. A.; and Stern, R. A.: Peculiarity of Shock Impingement on Area Convergence. *Phys. Fluids*, vol. 2, no. 4, July-Aug. 1959, pp. 427-431.
6. Rudinger, George: Passage of Shock Waves Through Ducts of Variable Cross Section. *Phys. Fluids*, vol. 3, no. 3, May-June 1960, pp. 449-455.
7. Rudinger, George: *Nonsteady Duct Flow—Wave-Diagram Analysis*. Dover Publ., Inc., c.1969.
8. Hertzberg, Abraham: A Shock Tube Method of Generating Hypersonic Flows. *J. Aeronaut. Sci.*, vol. 18, no. 12, Dec. 1951, pp. 803-804, 841.
9. Salas, M. D.: *Local Stability Analysis for a Planar Shock Wave*. NASA TP-2387, 1984.
10. Courant, R.; Friedrichs, K.; and Lewy, H.: Über die partiellen Differenzengleichungen der mathematischen Physik. *Math. Ann.*, vol. 100, 1928, pp. 32-74.

11. Roe, P. L.: Characteristic-Based Schemes for the Euler Equations. *Annual Review of Fluid Mechanics*, Volume 18, Milton van Dyke, J. V. Wehausen, and John L. Lumley, eds., Annual Reviews Inc., 1986, pp. 337–365.
12. Van Leer, Bram: Upwind-Difference Methods for Aerodynamic Problems Governed by the Euler Equations. *Large-Scale Computations in Fluid Mechanics, Volume 22—Part 2 of Lectures in Applied Mathematics*, Bjorn E. Engquist, Stanley Osher, and Richard C. J. Somerville, eds., American Mathematical Soc., 1985, pp. 327–336.

REPORT DOCUMENTATION PAGE			Form Approved OMB No. 0704-0188	
Public reporting burden for this collection of information is estimated to average 1 hour per response, including the time for reviewing instructions, searching existing data sources, gathering and maintaining the data needed, and completing and reviewing the collection of information. Send comments regarding this burden estimate or any other aspect of this collection of information, including suggestions for reducing this burden, to Washington Headquarters Services, Directorate for Information Operations and Reports, 1215 Jefferson Davis Highway, Suite 1204, Arlington, VA 22202-4302, and to the Office of Management and Budget, Paperwork Reduction Project (0704-0188), Washington, D.C. 20503.				
1. AGENCY USE ONLY (Leave blank)		2. REPORT DATE August 1991		3. REPORT TYPE AND DATES COVERED Technical Paper
4. TITLE AND SUBTITLE Shock Wave Interaction With an Abrupt Area Change			5. FUNDING NUMBERS 505-62-31-07	
6. AUTHOR(S) Manuel D. Salas				
7. PERFORMING ORGANIZATION NAME(S) AND ADDRESS(ES) NASA Langley Research Center Hampton, VA 23665-5225			8. PERFORMING ORGANIZATION REPORT NUMBER L-16878	
9. SPONSORING/MONITORING AGENCY NAME(S) AND ADDRESS(ES) National Aeronautics and Space Administration Washington, DC 20546-0001			10. SPONSORING/MONITORING AGENCY REPORT NUMBER NASA TP-3113	
11. SUPPLEMENTARY NOTES				
12a. DISTRIBUTION/AVAILABILITY STATEMENT Unclassified—Unlimited			12b. DISTRIBUTION CODE	
13. ABSTRACT (Maximum 200 words) <div style="display: flex; justify-content: space-between;"> <div> The wave patterns that occur when a shock wave interacts with an abrupt area change are analyzed in terms of the incident shock wave Mach number and area-jump ratio. The solutions predicted by a self-similar model are in good agreement with those obtained numerically from the quasi-one-dimensional time-dependent Euler equations. The entropy production for the wave system is defined and the principle of minimum entropy production is used to resolve a nonuniqueness problem of the self-similar model. </div> <div> Subject Category Q2 </div> </div>				
14. SUBJECT TERMS Shock wave interactions ; Area discontinuity ; Minimum entropy production			15. NUMBER OF PAGES 14	
			16. PRICE CODE A03	
17. SECURITY CLASSIFICATION OF REPORT Unclassified	18. SECURITY CLASSIFICATION OF THIS PAGE Unclassified	19. SECURITY CLASSIFICATION OF ABSTRACT	20. LIMITATION OF ABSTRACT	